**BNL-90850-2009-CP**

# *Investigations of Cadmium Manganese Telluride Crystals for Room-Temperature Radiation Detection*

**G. Yang, A.E. Bolotnikov, G.S. Camarda, Y. Cui, A. Hossain, K. Kim, V. Carcelen, R. Gul and R.B. James**

*Presented at the 2009 U.S. Workshop on the Physics and Chemistry of II-VI Materials*
Chicago, IL
October 6-8, 2009

December 2009

**Nonproliferation and National Security Department**
**Detector Development and Testing Division**

**Brookhaven National Laboratory**
P.O. Box 5000
Upton, NY 11973-5000
www.bnl.gov

# DISCLAIMER

# INVESTIGATIONS OF CADMIUM MANGANESE TELLURIDE CRYSTALS FOR ROOM-TEMPERATURE RADIATION DETECTION

G. YANG[1,4], A. E. BOLOTNIKOV[1], G. S. CAMARDA[1], Y. CUI[1], A. HOSSAIN[1], K.KIM[1], V. CARCELEN[1,2], R. GUL[1,3], and R. B. JAMES[1]

1. Brookhaven National Laboratory, Upton, NY 11973, USA.

2. Laboratorio de Crecimiento de Cristales, Dpto. Fisica de Materiales, Facultad de Ciencias, University Autonoma de Madrid, 28049 Madrid, Spain.

3. Idaho State University, Pocatello, ID 83209, USA.

4. email: gyang@bnl.gov

## Abstract

Cadmium manganese telluride (CMT) has high potential as a material for room-temperature nuclear-radiation detectors. We investigated indium-doped CMT crystals taken from the stable growth region of the ingot, and compared its characteristics with that from the last-to-freeze region. We employed different techniques, including synchrotron white-beam X-ray topography (SWBXT), current-voltage (I-V) measurements, and low-temperature photoluminescence spectra, and we also assessed their responses as detectors to irradiation exposure. The crystal from the stable growth region proved superior to that from the last-to-freeze region; it is a single-grain crystal, free of twins, and displayed a resistivity higher by two orders-of-magnitude. The segregation of indium dopant in the ingot might be responsible for its better resistivity. Furthermore, we recorded a good response in the detector fabricated from the crystal taken from the stable growth region; its $(\mu\tau)_e$ value was $2.6 \times 10^{-3}$ $cm^2/V$, which is acceptable for thin detectors, including for applications in medicine.

**Keywords:** CMT, synchrotron white-beam X-ray topography, photoluminescence spectra, detector response, twins

## Introduction

Cadmium manganese telluride (CMT) is a diluted magnetic compound semiconductor, previously used in Faraday rotators, optical isolators, solar cells, lasers, magnetic field sensors, and infrared detectors [1, 2]. Recent researchers demonstrated the great potential of CMT for applications in room-temperature radiation detection. Compared to the widely investigated cadmium zinc telluride (CZT), CMT offers some distinct advantages that make it a good candidate to compete with CZT in such applications. First, the segregation coefficient of Mn in CdTe is nearly unity, while that of Zn in CdTe has a coefficient of 1.35 [3]. This difference accounts for the nearly uniform concentration of Mn in CdTe, compared to the high variation of Zn concentration in CdTe. This superior compositional homogeneity of CMT might well enhance the yield of suitable crystals for detectors, and ultimately, lower costs of producing large-area arrays. Furthermore, CMT displays greater tunability of its band gap because of the large compositional influence of Mn. Thus, adding Mn increases the room-temperature band gap at a rate of 13 meV/[%Mn], i.e., an increase more than twice as large as that obtained after adding Zn to CdTe [4]. A band-gap in the range of 1.7-2.2 eV has proven ideal for assuring an optimal signal/noise ratio in X-ray and gamma-ray detectors [5]; such optimization can be attained by adding relatively less Mn. This advantage lessens the impact of the many alloying-related problems related to this material. However, a lack of high-quality material currently limits the development of CMT detectors. Recently, our group at Brookhaven National Laboratory, in collaboration with Yinnel Tech, Inc., has investigated properties of indium-doped CMT crystals by employing different techniques, such as synchrotron white-beam X-ray topography (SWBXT), current-voltage (I-V) characteristic measurement, low-temperature photoluminescence spectra, and the response of the fabricated detectors. Here, we report our results from assessing the crystallinity quality of CMT crystals, and their opto-electrical properties; also, we detail our findings on their performance as radiation detectors.

**Experimental**

CMT crystals doped with indium were grown with the modified low-pressure Bridgman method (MLB) by Yinnel Tech, Inc. The manganese mole fraction in the CMT ingot was ~0.05. In an as-grown ingot, large single crystals usually can be obtained from the stable growth region, and from the last-to-freeze region; together, these regions occupy about 85% volume of the entire ingot, while the first-to-freeze region acts as a competitive nucleation portion, and is made up of multi-crystals. In this work, we chose one crystal from the stable growth region and one from the last-to-freeze region of the ingot for our comparison. The crystals measured 10 x10 x 2 $mm^3$. After cutting them from the ingot with a wire saw, we lapped them with 5-μm grit $Al_2O_3$ abrasive papers, polished their surfaces with a 0.05-μm particle-size alumina suspension, and then rinsed them in methanol. After removing the mechanically damaged layers from the crystals' surfaces with 2% bromine-methanol solution, the Au-CZT electrodes were prepared on the top and the bottom surfaces of the crystals by electroless chemical deposition.

We conducted the SWBXT experiments with reflection geometry at the X19C beamline of the National Synchrotron Light Source (NSLS) at Brookhaven National Laboratory. A white X-ray beam from synchrotron radiation, with a spot size of 15 mm x 7 mm, covered the samples, and a highly sensitive film (Kodak Industries, SR 45, Rochester, NY), providing a spatial resolution of 1 μm, was employed to collect the diffraction signals. The corresponding diffraction patterns obtained contain large-area diffraction spots with good spatial-resolution. Each spot is an x-ray topograph, constituting a map of the diffracting power as a function of position in the crystal. The small ratio between the source's dimension and the source distance ensures the high resolution of the approach.

I-V characteristics were measured with a Keithley 237 voltage source-measure unit controlled by an external computer. For the photoluminescence measurement, we attached the crystals with grease to a cold copper finger in an open-cycle cryostat to keep the sample's temperature at 9 K.

An argon laser operating at 488 nm was used to excite the photoluminescence spectrum, while a Princeton Instrument SpectraPro 2500i spectrometer collected and analyzed the signals emitted from the samples. In addition, we measured the ability of these CMT crystals to detect irradiation from an alpha source (Am-241).

**Results and discussion**

We characterized the crystalline quality of CMT crystals by the SWBXT measurements with the reflection geometry. Fig. 1 shows the topography of the crystal from the stable growth region. It is a single-grain one, free throughout of large-scale defects, such as twin boundaries. At the same time, we observed some localized cellular-network structures within it, whose formation we attributed to polygonization, i.e., the stress-induced glide and climb of dislocations introduced in the crystal during solidification [6, 7]. The dislocations produce a strain field in the surrounding regions; consequently, leading to an enhanced intensity compared with the rest of the crystal [8]. Accordingly, diffraction contrast is generated, revealing the dislocations and strained regions inside the crystal. The presence of the cellular-like structures signifies that the dislocations propagate and connect with each other in these localized regions. In support of this interpretation, we found evidence of slipped bands near the cell structures, caused by dislocation-induced stresses in these regions. Fig. 2 shows the topography of the crystal from the last-to-freeze region. The most obvious feature is the extension of several lamellar twins across the whole crystal, easily revealed by the contrast in orientation. The reason for their occurrence is that the magnitude of thermal stress is higher in the last-to-freeze region of the ingot due to the change of thermal environment at the growth interface (heat flow is transferred from solidified crystals to the Cd vapor instead of from the crystals to the melt). The relatively high ionicity of CMT makes it prone to twinning when stress is high. Furthermore, the last-to-freeze material exhibits a distortion of the lattice on one side (blurry side), confirming the change of thermal stress in this portion of the ingot. We note that there are fewer cellular-like structures in the crystal from the

last-to-freeze region. Possibly, twin boundaries act as a barrier to the propagation of dislocations [9-10].

Fig. 3 gives the I-V curves of the CMT crystals. The corresponding resistivity was $2.0 \times 10^{10}$ Ω-cm for the crystal from the stable growth region, two orders-of-magnitude higher than that of the crystal from the last-to-freeze region. It is interesting to clarify this phenomenon since both crystals are from the same ingot. Therefore, we further measured the low-temperature photoluminescence spectra of the CMT crystals, as illustrated in Fig. 4. These spectra can be divided into three regions: Near-band-edge region consisting of the donor-bound exciton ($D^0$,X) peak and the acceptor-bound ($A^0$,X) peak; donor–acceptor pair (DAP) recombination region; and, defect-related region associated with some impurity-complex energy levels ($D_{complex}$). Comparing these curves, the exciton peaks dominate the whole spectra for the crystal from the stable middle portion of the ingot, while the $D_{complex}$ peak is the main peak in the CMT crystal from the tail portion. Due to the high partial pressure of the Cd component during the growth of CMT ingots by MLB, a large number of cadmium atoms escape, leaving many cadmium vacancies ($[V_{Cd}]^{2-}$) in the as-grown crystal. These cadmium vacancies usually act as shallow acceptors. When the CMT material is doped with indium, the indium atoms can form a complex with the cadmium vacancies and act as donors. After ionization, an electron is provided, and a donor ion, $[In_{Cd}]^{+}$, is formed. Two $[In_{Cd}]^{+}$ attract one $[V_{Cd}]^{2-}$ and create a neutral complex, $2[In_{Cd}]^{+}$–$[V_{Cd}]^{2-}$. The In-related complex generates the $D_{complex}$ peak in the photoluminescence spectra. Therefore, the increasing intensity of the $D_{complex}$ peak indicates that there is more indium in the last-to-freeze region of CMT ingot. This finding is explained by the fact that indium preferentially accumulates towards the ingot tail due to its segregation coefficient of 0.075 in CMT [11]. Furthermore, some extra indium atoms might become interstitial atoms in the tail portion after the cadmium vacancies are fully compensated, providing a higher carrier- (electron) density. Thus, the resistivity will be reduced. Impurities with segregation coefficients less than 1 may also play a role.

We used an alpha source (Am-241) for measuring performance of both CMT detector crystals. The crystal from the last-to-freeze region gave no response; this might be attributed to its low resistivity. Another possibility is that the twin boundaries in this crystal acted as conductive channels, resulting in a high leakage current when the bias voltage was applied. In contrast, the typical peak of 59.5 keV for Am-241 readily is distinguishable in the CMT crystal from the stable growth portion of the ingot (Fig. 5). Fig. 6 plots its charge collection as a function of applied bias voltage. The carrier-mobility characteristics were calculated by the fitting the above data to the single-carrier Hecht equation,

$$Q(V) = \frac{qVN_0(\mu\tau)_e}{d^2}[1 - \exp(\frac{d^2}{(\mu\tau)_e V})] \quad [1]$$

where $N_0$ is the number of carriers created by the incident radiation, $Q$ the total charge collected, $\mu$ the carrier mobility, $\tau$ the carrier lifetime, $d$ the distance between the anode and cathode, $q$ the electron charge, and $V$ is the applied bias voltage. The extracted $(\mu\tau)_e$ value is $2.6 \times 10^{-3}$ $cm^2/V$, which is acceptable for thin detectors in medical and other applications.

**Conclusions**

In summary, we investigated indium-doped CMT crystals from the stable growth region and the last-to-freeze region employing different techniques, including synchrotron white-beam X-ray topography (SWBXT), current-voltage (I-V) characteristic measurement, low-temperature photoluminescence spectra, and finally the detector response to irradiation. The crystal from the stable growth region is superior to that taken from the last-to-freeze region. It is a single-grain crystal, free from twins, and has a higher resistivity. The segregation of indium might be responsible for improving its resistivity. This crystal, configured as a detector, gave a satisfactory response to irradiation. The corresponding $(\mu\tau)_e$ value was $2.6 \times 10^{-3}$ $cm^2/V$, quite acceptable for thin detectors in medical applications.

**Acknowledgments**

We would like to acknowledge Dr. Zhenxian Liu and Dr. Balaji Raghothamachar for their kind help during the photoluminescence measurements at U2A beamline of NSLS and SWBXT experiments at X19C beamline of NSLS at Brookhaven National Laboratory. This work was supported by US Department of Energy, Office of Nonproliferation Research and Development, NA-22. The manuscript has been authored by Brookhaven Science Associates, LLC under Contract No. DE-AC02-98CH1-886 with the U.S. Department of Energy. The United States Government retains, and the publisher, by accepting the article for publication, acknowledges, a worldwide license to publish or reproduce the published form of this manuscript, or allow others to do so, for the United States Government purposes.

**References**

[1] G.A. Brost, K. M. Magde and S. Trivedi, *Opt. Mater.* 4, 224 (1995).

[2] U. Hommerich, X. Wu, V. R. Davis, S. B. Trivedi, K. Grasza, R. J. Chen and S. Kutcher, *Opt. Lett.* 22, 1180 (1997).

[3] A. Tanaka, Y. Masa, S. Seto and T. Kawasaki, *J. Crystal Growth* 94, 166 (1989).

[4] D. J. Olego, J. P. Faurie, S. Sivananthan and P. M. Raccah, *Appl. Phys. Lett.* 47, 1172 (1985).

[5] J. T. Toney, T. E. Schlesinger and R. B. James, *IEEE Trans. Nucl. Sci. A* 428, 14 (1999).

[6] S. McDevitt, B. E. Dean, D. G. Ryding, F. J. Scheltens and S. Mahajan, *Mater. Lett.* 4, 451 (1986).

[7] D. J. Williams and A. W. Vere, *J. Cryst. Growth* 83, 341 (1987).

[8] B. Raghothamachar, H. Chung, M. Dudley and D.J. Larson, Jr., *J. Electron. Mater.* 27, 556 (1998).

[9] H. Chung, B. Raghothamachar, M. Dudley and D. J. Larson, Jr., *SPIE* 2809, 45 (1996).

[10] W. Zhou, M. Dudley, J. Wu, C. H. Su, M. P. Volz, D. C. Gillies, F. R. Szofran and S. L. Lehoczky, *Mater. Sci. & Eng. B* 27, 143 (1994).

[11] Jijun Zhang, Wanqi Jie, Tao Wang, Dongmei Zeng and Bo Yang, *J. Cryst. Growth* 306, 33 (2007).

**Figure Captions**

Fig. 1 Topography of a CMT crystal from the stable growth region

Fig. 2 Topography of a CMT crystal from the last-to-freeze region

Fig. 3 I-V curves of CMT crystals from the stable growth region and from the last-to-freeze region

Fig. 4 . Low-temperature photoluminescence spectra of CMT crystals from the stable growth region and from the last-to-freeze region

Fig. 5 Energy spectrum of the CMT crystal from the stable growth region (A sealed source Am-241 was used in the measurement).

Fig. 6 Plot of charge collection as a function of applied bias voltage in the crystal from the stable growth region

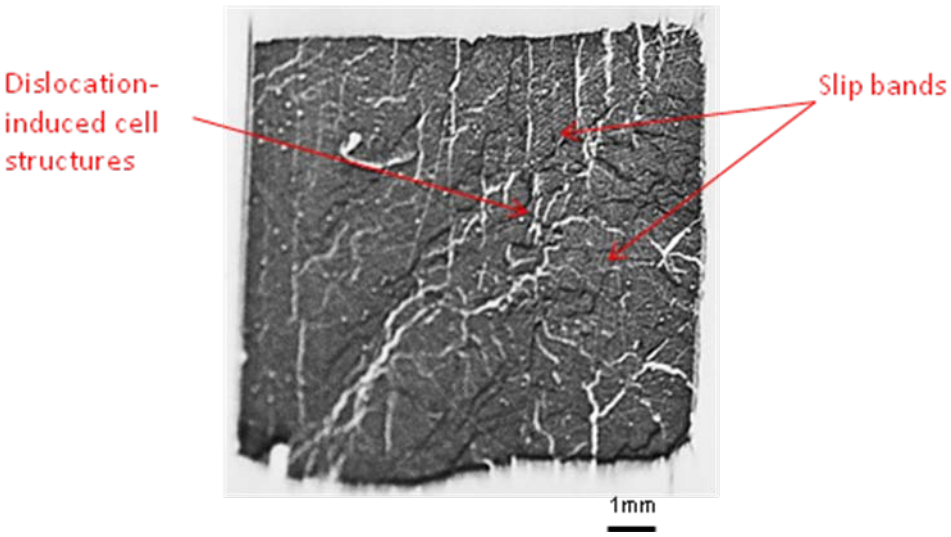


Fig. 1 Topography of a CMT crystal from the stable growth region

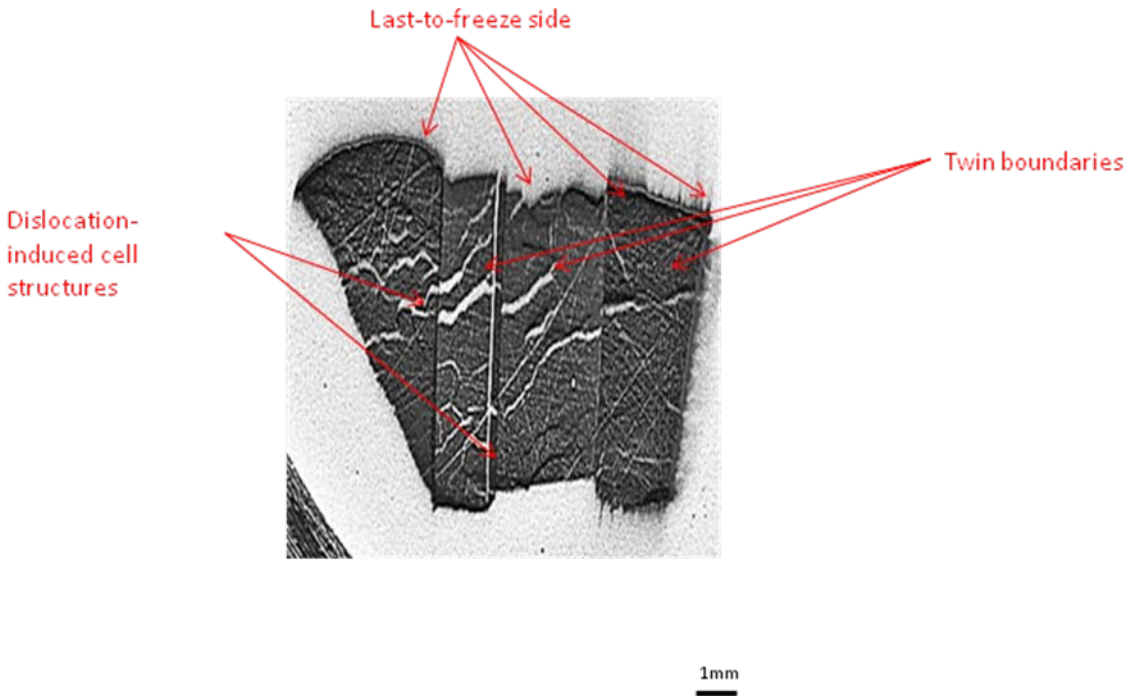


Fig. 2 Topography of a CMT crystal from the last-to-freeze region

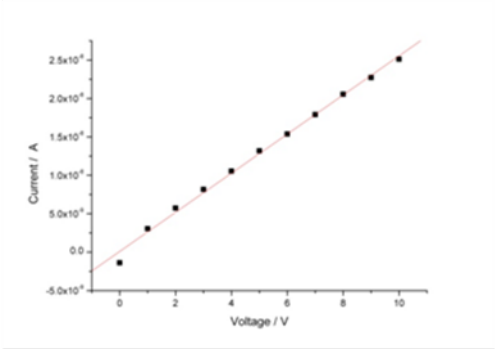


Crystal from the stable growth region

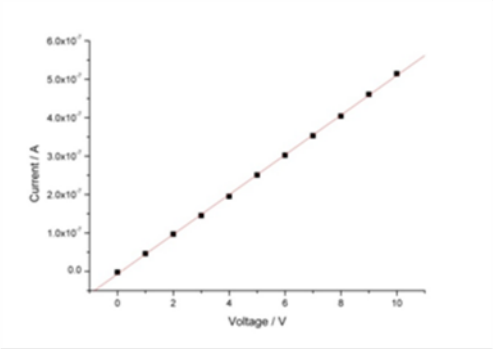


Crystal from the last-to-freeze region

Fig.3 I-V curves of CMT crystals from the stable growth region and from the last-to-freeze region

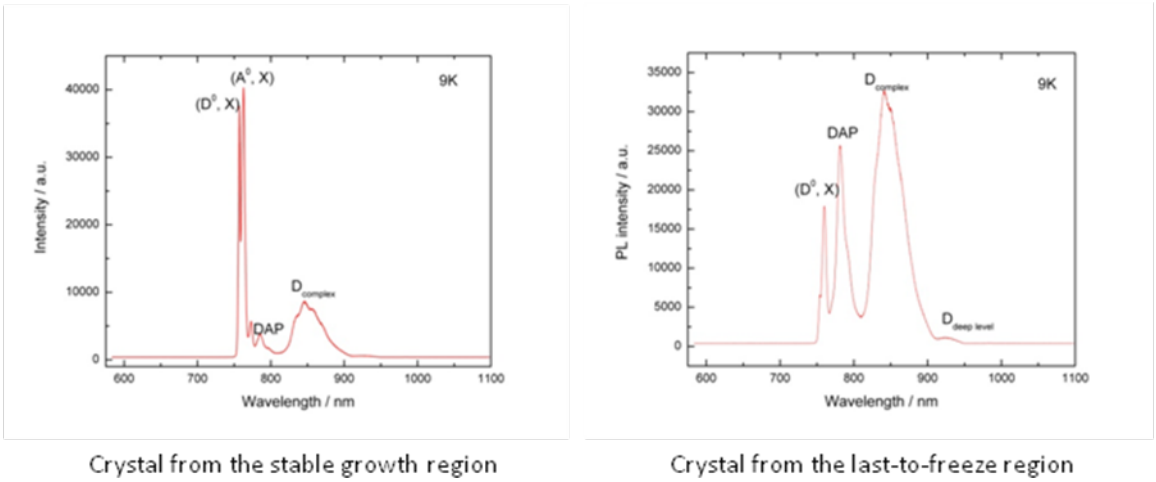


Fig. 4. Low-temperature photoluminescence spectra of CMT crystals from the stable growth region and from the last-to-freeze region

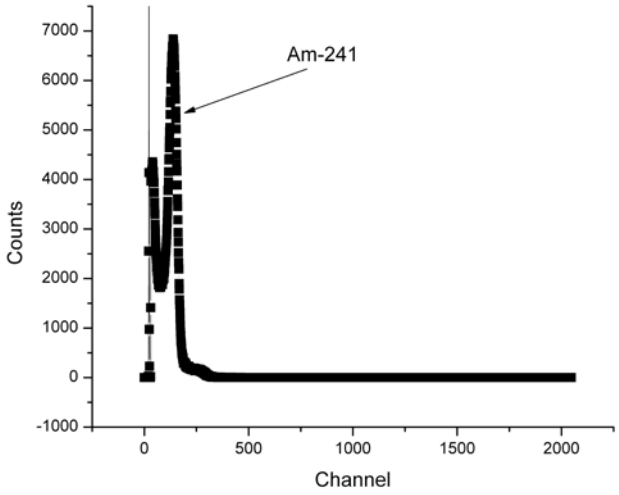


Fig. 5 Energy spectrum of the CMT crystal from the stable growth region (A sealed source Am-241 was used in the measurement).

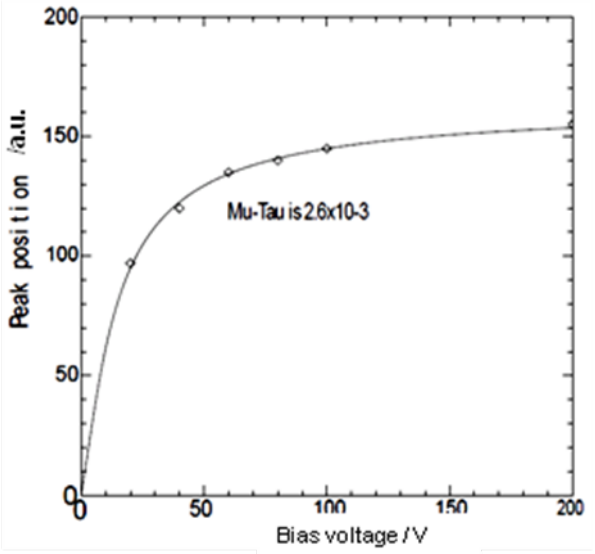


Fig. 6 Plot of charge collection as a function of applied bias voltage in the crystal from the stable growth region